JOURNAL OF MATERIALS SCIENCE **36** (2001) 5253–5263

Sol-gel-derived hydroxyapatite powders and coatings

E. TKALCEC*,‡, M. SAUER, R. NONNINGER, H. SCHMIDT
Institut fuer Neue Materialien, Im Stadtwald, Gebaeude 43, D-66123 Saarbruecken, Germany
E-mail: etkalcec@pierre.fkit.hr

Hydroxyapatite (HAP) and tri-calcium phosphate (TCP) powders and coatings with a Ca/P molar ratio from 1.56 to 1.77 were prepared by the sol-gel technique using calcium 2-ethylhexanoate ($Ca(O_2C_8H_{15})_2$) and 2-ethyl-hexyl-phosphate as calcium and phosphorus precursors, respectively. The structural evolution and phase formation mechanisms of HAP and tri-calcium phosphate in calcined powders and coatings on Si wafer and Ti-alloy substrates (Ti-30Nb-3Al and Ti-5Al-2.5Fe) were characterized by X-ray diffraction, Fourier transform infrared spectroscopy (FTIR) and scanning electron microscopy (SEM). The elimination of organics was studied by differential thermal analysis (DTA) and thermogravimetry (TGA). Two different formation mechanisms of crystallization are proposed. In sols with Ca/P $\leq$ 1.67, β-tricalcium phosphate is formed as the major phase and hydroxyapatite as a minor phase by calcination at 700°C. At 900°C these phases react to form AB-type carbonated hydroxyapatite ($Ca_{10-2x/3}[(PO_4)_{6-x}(CO_3)_x][(OH)_{2-x/3-2y}(CO_3)_y]$). A release of CO_2 substituting PO_4^{3-} occurs between 900°C and 1100°C yielding carbonate apatite, $Ca_{10}(PO_4)_6[(OH)_{2-2y}(CO_3)_y]$, whereas CO_2 substituting OH^- groups in the apatite structure is released above 1200°C. In sols with Ca/P $\geq$ 1.70, rather than carbonate apatite, B-carbonated hydroxyapatite $Ca_{10-2x/3}[(PO_4)_{6-x}(CO_3)_x](OH)_2$ is formed, which subsequently decomposes into HAP and CaO above 1200°C. The optimum sintering conditions for coatings on Ti-alloys are found to be 600°C for 10 minutes, since, at higher temperature, oxidation of titanium and the formation of rutile (TiO_2) occur. Dip coating and sintering in two cycles yielded a homogeneous and dense coated film with a thickness of 250 nm.

1. Introduction

Hydroxyapatite bioceramic (HAP) ($Ca_{10}(PO_4)_6(OH)_2$) has attracted world-wide interest in both the orthopaedic [1] and dental fields [2], owing to its excellent biocompatibility and tissue bioactivity. Because of the low fracture toughness and modulus of elasticity of HAP ceramics [3], their application is generally restricted to non-load-bearing areas, unless combined with other materials offering greater mechanical properties. Therefore, nearly all bone and tooth implants are presently made from metal alloys coated with HAP to improve the rate of implant fixation and prolong its longevity. The concept of coating metal implant surfaces with HAP ceramic films combines the mechanical benefits of metal alloys with the biocompatibility of HAP. Commercial HAP coatings, commonly produced by plasma spraying [4, 5], have been shown to exhibit clinical problems such as delamination, which leads to the premature wear of implants [6]. To improve adhesion between coatings and implants, new synthetic approaches are currently being developed, such as sputtering [7], pulsed-laser deposition [8], thermal dissociation of calcium-EDTA chelates under hydrothermal conditions [9], biomimetic processes [10] and liquid immersion techniques [11, 12]. The sol-gel process provides an attracive alternative to these methods. It has been widely used in the preparation of various inorganic materials because of the easy formation of crystalline films at relatively low temperature, the possibility to tailor microstructures and its convenience for complex-shape coatings [13]. In the sol-gel process, the metal alkoxides $M(OR)_n$ used as starting materials are converted through hydrolysis and condensation reactions to amorphous gels of metal oxides, which are further transformed to ceramics when heated at relatively low temperatures.

Calcium phosphate compounds such as hydroxyapatite ($Ca_{10}(PO_4)_6(OH)_2$), or tri-calcium phosphate ($Ca_3(PO_4)_2$, (TCP)) have only recently been synthesized by sol-gel processes as bulk powders [14, 15] or as coatings [16, 17]. Brendel *et al*. [16] prepared HAP by the so-called polymeric route using calcium nitrate

*Author to whom all correspondence should be addressed.
‡*Present Address:* Faculty of Chemical Engineering and Technology, University of Zagreb, Croatia.

and phenyldichlorophosphine ($C_6H_5PCl_2$) as precursors and acetone as a solvent. Hydrolysis and subsequent oxidation with bubbling air led to the formation of the viscous sol used for coating metal substrates. The sol transforms into a rigid gel upon drying and to hydroxyapatite upon calcination at 900 to 1000°C. Weng and Baptista [18] used P_2O_5 dissolved in ethanol as the phosphorus precursor and calcium nitrate as the calcium precursor. The latter authors pointed out that the alcoholic solution of P_2O_5 contains the P species mainly in the form of $PO(OH)_2(OR)$ and $PO(OH)(OR)_2$, which hydrolyse faster than $PO(OR)_3$. Lopatin *et al*. [19] and Russell *et al*. [20] used n-butyl acid phosphate and calcium nitrate tetrahydrate as the phosphorus and calcium sources, respectively. The reaction was performed at room temperature in a solvent of 2-methoxyethanol. Sauer *et al*. [21] recently prepared coatings on Ti-alloys using sol-gel derived hydroxyapatite infiltrated in surface-modified HAP particles.

In this paper, we describe the preparation of calcium phosphate powders and coatings using calcium 2-ethylhexanoate ($Ca(O_2C_8H_{15})_2$) as the calcium precursor and 2-ethyl-hexyl-phosphate as the phosphorus precursor. Si-wafer and Ti-alloy substrates (Ti-30Nb-3Al and Ti-5Al-2.5Fe) were dip coated with obtained stable sols. Both organic precursors were used by Hosonuma *et al*. [22] for the preparation of calcium phosphate coatings on titanium, titanium alloys and stainless steel alloys. The authors [22] pointed out that the coatings may contain, in addition to hydroxyapatite and/or tricalcium phosphate, other calcium phosphates formed as by-products of the firing process or coatings-substrate reactions. Therefore, the aim of this work was to study the formation mechanism of the crystalline phases in the firing processes of coatings with different Ca/P molar ratios. Special attention was devoted to the incorporation of CO_2 in the apatite structure, since carbonate apatite closely resembles the mineral phase of bone and gained recently considerable attention due to enhanced dissolution and resorption properties [23].

2. Experimental procedure

2.1. Sol-gel synthesis and coating procedure

2.1.1. Preparation of sols

74 g of calcium hydroxide (98%, Merck, GmbH) was suspended in 150 ml ethanol (>99% Fluka, GmbH) and stirred vigorously. To this suspension 433.5 g ethylhexanoic acid (EHA) was added dropwise. The molar ratio of calcium to EHA equaled 1 : 3. The suspension was stirred for another 3 h at 50°C, then cooled to room temperature and diluted with 90 ml ethanol to reduce the viscosity of the solution. The turbid solution was then filtered by pressure filtering (pore diameter 2 μm) to obtain a clear solution of calcium 2-ethylhexanoate. The amount of Ca was determined by ICP-AES to be 5.67 wt%. The CaEHA-solution was subsequently diluted with EHA to a Ca/EHA molar ratio of 1 : 8. 2-ethylhexyl-phosphate (99.2 wt%, Merck, GmbH, mixture of 45% mono- and 55% di-ester of phosphoric acid) was added in various amounts to obtain solutions with Ca/P molar ratios of 1.60, 1.67, 1.70, 1.75 and 1.80. After adding ethanol to reduce the overall calcium phosphate concentration to 5 wt%, the solutions were stirred at 25°C for 4 h before being used for coating. Furthermore, sols were dried at 130°C for 4 h and the resulting gels were heat treated at temperatures in the range from 400 to 1400°C.

2.1.2. Coating procedure

Ti-alloys and single-crystal silicon wafers were coated with prepared sols. Circular titanium-alloy plates (Ti-30Nb-3Al and Ti-5Al-2.5Fe) with 15 mm diameter and 1 mm thickness were polished with 15 μm diamond paste, cleaned in an ultrasonic bath, washed with distilled water and acetone and dried at 80°C before coating. Si wafers (20 × 10 mm) were rinsed in acetone and dried at 80°C.

Coating was performed by dipping the substrates into sols at 25°C, and pulling them out with a speed of 1 mm/s, drying them in air at 130°C for 4 h and subsequently calcining them for 10 minutes in a preheated furnace at temperatures between 400 and 900°C.

2.2. Characterization of sols and coatings

Elemental analysis of dried and calcined gels was carried out using ICP-AES (ISA, JY24). Thermal behaviour and phase analyses were accomplished by differential thermal and thermogravimetric analyses (DTA/TGA) (Baer, Model STA-501, heating rate: 10 K min^{-1}), X-ray diffraction analysis (XRD) (Siemens D5000, Cu K_α radiation) and by Fourier transform infrared spectroscopy (FTIR) in transmission mode (Brucker IFS25). For the phase characterization of coatings on substrates by XRD, a thin-film accessory was used at an offset angle $\theta = 1.5°$. FTIR analyses were performed on powders prepared by the KBr-pellet technique (KBr/samples = 150/1) and on coatings deposited on Si single-crystal wafers (thickness of Si wafer = 500 μm). The microstructure and morphology of coatings on Si wafers and Ti-alloys were determined by scanning electron microscopy (JEOL, JSM 6400F).

3. Results

A flow chart of sol preparation and substrate coating is given in Fig. 1. Sample notation and both nominal and determined Ca/P molar ratios of prepared sols are given in Table I.

TABLE I Sample notation and nominal and measured Ca/P molar ratios of sols

Gel	Nominal Ca/P molar ratio of sols	Measured (ICP) Ca/P ratio of gels calcined at 1000°C
EHP1	1.60	1.55
EHP2	1.64	1.59
EHP3	1.67	1.62
EHP4	1.70	1.66
EHP5	1.75	1.70
EHP6	1.80	1.77

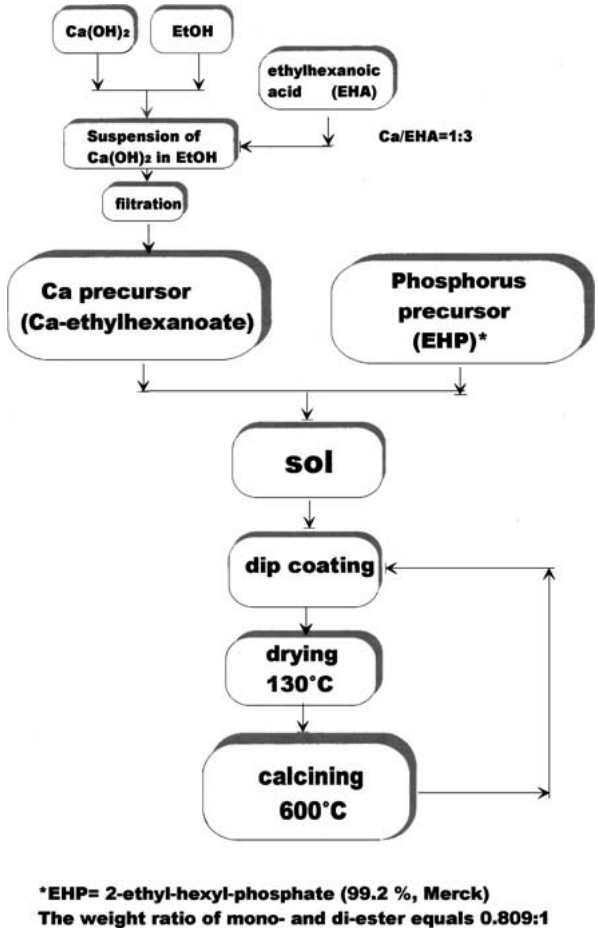

Figure 1 Flow chart of sol synthesis and substrate coating.

3.1. Thermal behavior of prepared sols

Prepared sols dried at 130°C transformed in 4 hours into transparent sticky gels. The latter were subjected to differential thermal (DTA) and thermogravimetric (TGA) analyses. DTA/TGA scans of the EHP3 gel (Ca/P = 1.62) dried at 130°C for 4 hours (Fig. 2) are typical for the thermal analyses performed on these samples.

The first weak endothermic peak seen in the DTA scan at about 260°C can be attributed to the evaporation of residual solvent, while the subsequent strong exothermic peak at about 400°C results from the combustion of organic material. The weight loss seen in the corresponding TGA scan is 73.05% at 500°C, and between 500°C and 1490°C the gel lost a further 1.20% of its original weight. Additionally, small exothermic peaks are observed in the DTA scan at 512, 582 and 1199°C (see overlay in Fig. 2). To define these peaks with certainty, the majority of organic material was burned off at 400°C for 5 minutes, and the rest of powder was again subjected to thermal analysis.

In this case, the heating of the sample was stopped successively at higher temperatures and the sample was rapidly cooled down and analysed by XRD. DTA/TGA and differentiated TGA (DTGA) scans of EHP3 gel calcined at 400°C for 5 min. are shown in Fig. 3, and XRD patterns of samples quenched in the DTA apparatus from the indicated temperatures are displayed in Fig. 4.

While the sample quenched from 400°C is still amorphous, at 535°C β-tri-calcium phosphate (β-TCP)

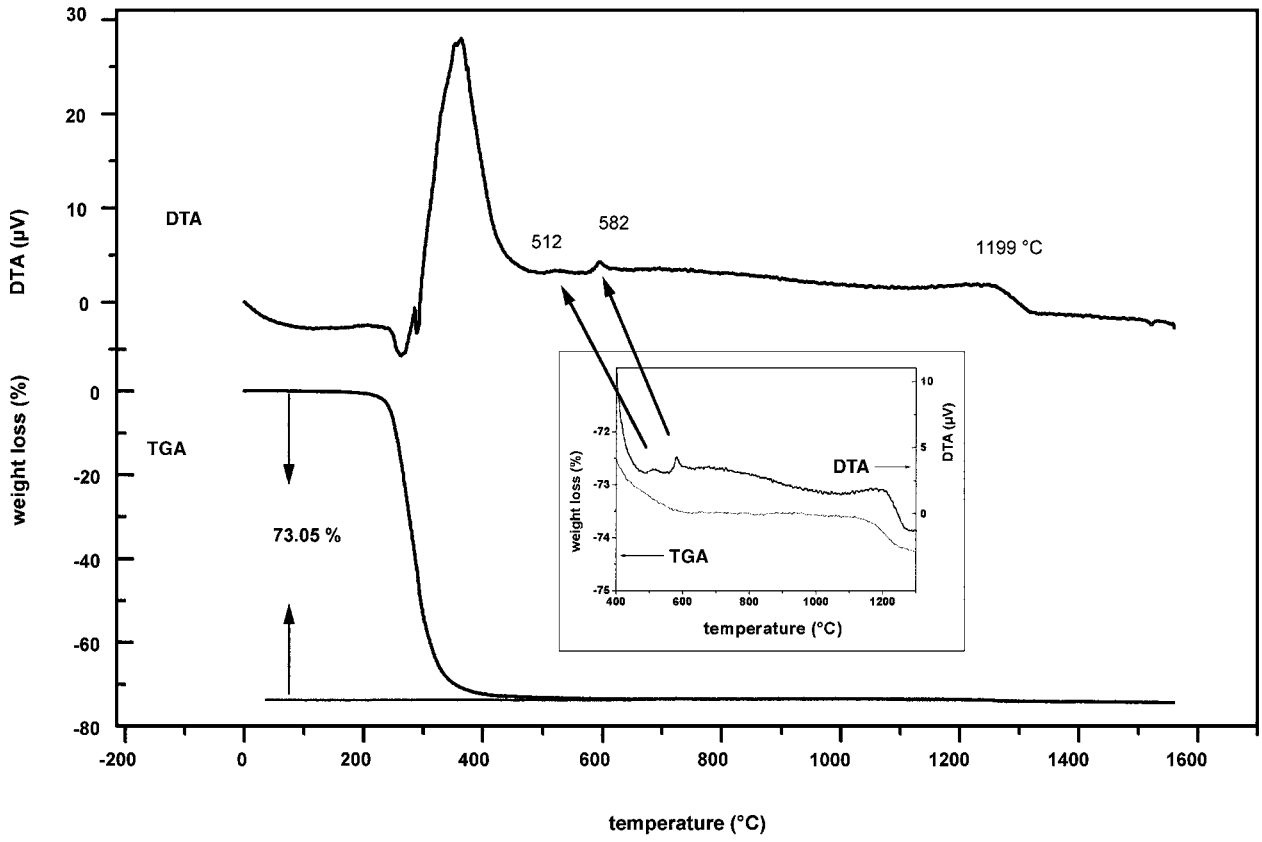

Figure 2 Differential thermal and thermogravimetric analyses (DTA/TGA) of a gel with Ca/P = 1.62 (EHP3) dried at 130°C for 4 h. (DTGA = differentiated TGA).

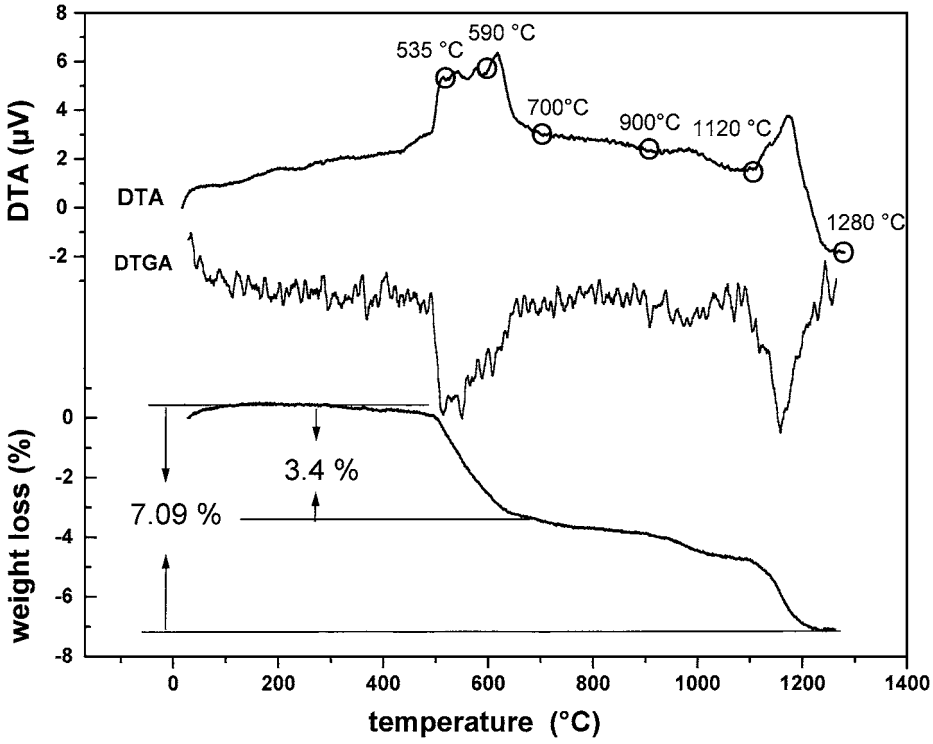

Figure 3 Differential thermal and thermogravimetric analyses (DTA/TGA) of sol EHP3 (Ca/P = 1.62) calcined at 400°C for 5 minutes.

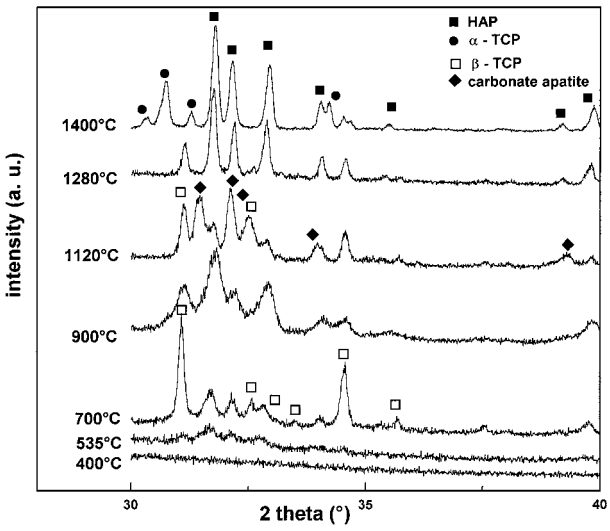

Figure 4 XRD patterns of the gel with Ca/P = 1.62 (EHP3) quenched from temperatures marked in Fig. 3. (—□—) β-TCP; (—■—) hydroxyapatite; (—◆—) carbonate apatite, (—●—) α-TCP.

and hydroxyapatite (HAP) begin to crystallize, and at 700°C the former is the predominant phase, and the latter a minor one. A third crystalline phase, carbonate apatite ($Ca_{10}(PO_4)_6CO_3$) appeared at 1120°C, but was absent in the sample quenched from 1280°C, in which only well-crystallized HAP and β-TCP were observed. The latter transforms into α-TCP above 1280°C, resulting in a mixture of well crystallized HAP and α-TCP in the sample heated to 1400°C.

The same crystallization path was observed in the other gels having Ca/P $\leq$ 1.66 (EHP1, EHP2 and EHP4). However, a different crystallization path was found in the gels with Ca/P $\geq$1.70. XRD patterns of the gel with Ca/P = 1.77 (EHP6) quenched from various temperatures in the DTA apparatus are given in Fig. 5. The first crystalline phase to form is HAP with β-TCP appearing as minor phase at 700°C. No carbonate apatite appears as a distinct phase, but at 1060°C some splitting of HAP peaks is observed. At 1280°C and 1500°C, in addition to HAP, a small amount of CaO was found. A segment of the XRD pattern between 30–35° 2θ is shown in Fig. 5B for the sample quenched at 1060°C. The theoretical 2θ peak positions of HAP and carbonate apatite are also included.

Further evidence for the formation of carbonate apatite as a separate phase in the gels with molar ratio Ca/P $\leq$ 1.66 is found in XRD patterns of gels heat treated at 1000°C for 3 hours (Fig. 6a–d). Comparing the XRD patterns of the same gel subjected to two different heat treatments (Fig. 6b and c), we see that pre-treatment of the sample has a decisive influence on carbonate apatite formation.

FTIR spectra corresponding to the XRD patterns of Fig. 4 are displayed in Fig. 7. The spectrum at 400°C exhibits featureless bands at 1060 cm^{-1} and 570 cm^{-1}, which can be assigned to non-separated ν_1 and ν_3 vibrations, and to ν_4 vibration modes of PO_4^{3-} groups, respectively [24]. The FTIR spectrum indicates an amorphous state [25] of the gel at 400°C. Absorption bands in the range of 1400 to 1570 cm^{-1} can be attributed to C–O and C=O stretching vibrations of organic residuals. Bands at 3400 and 1634 cm^{-1} arise from adsorbed molecular water. As the temperature increases, the absorption bands resulting from P–O deformation (570, 601 cm^{-1}) and valence vibrations (1046, 1090 cm^{-1}) separate and become stronger and sharper. The band at 1419 cm^{-1}, which could be due to CO_2 incorporation at the PO_4^{3-} position in the apatite structure, becomes

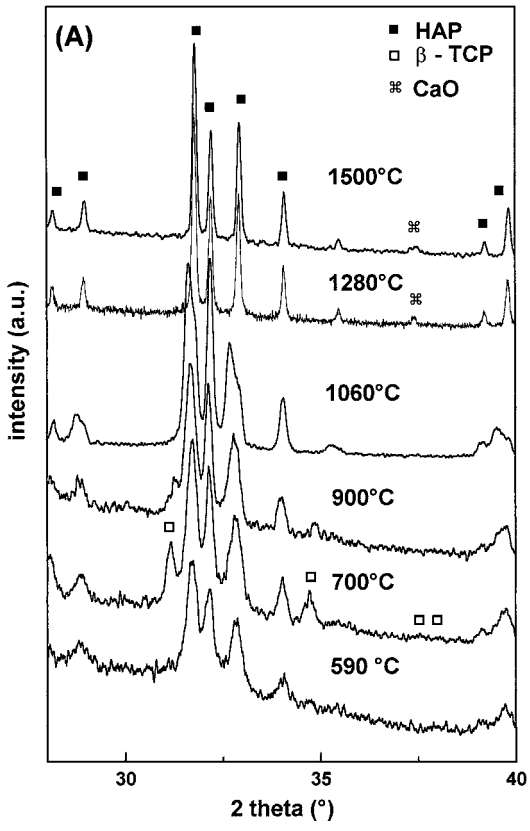

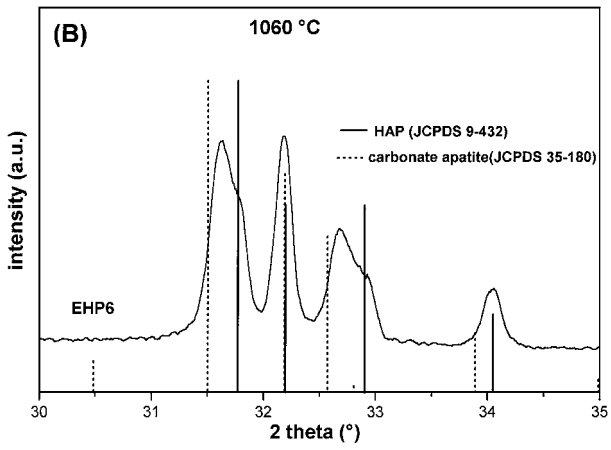

Figure 5 (A) XRD patterns of the gel with Ca/P = 1.77 (EHP6 gel) quenched in the DTA apparatus from the indicated temperatures; (B) a segment of the XRD pattern between 30–35° 2θ and the theoretical positions of HAP and carbonate apatite peaks in the given range.

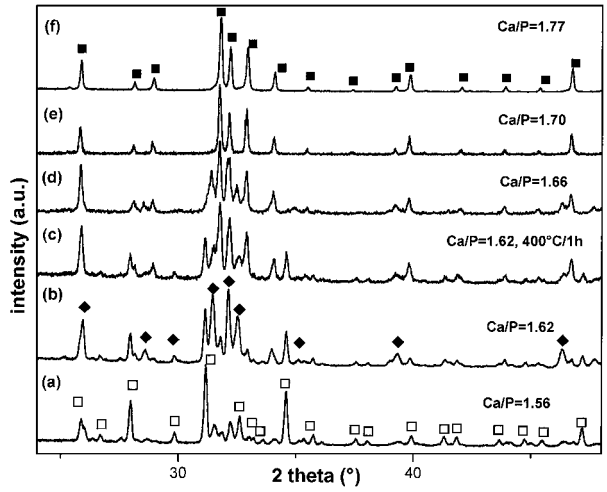

Figure 6 XRD patterns of gels with various Ca/P molar ratio: (a) Ca/P = 1.56, (b) Ca/P = 1.62, (d) Ca/P = 1.66, (e) Ca/P = 1.70 and (f) Ca/P = 1.77 heat-treated at 1000°C for 3 hours, and (c) Ca/P = 1.62 pre-heated at 400°C, cooled down to room temperature and treated in a second step at 1000°C for 3 hours. (—□—) β-TCP; (—■—) hydroxyapatite; (—◆—) carbonate apatite.

intense at 700°C. At 900°C, the bands at 1545, 1460 and 1419 cm^{-1} attributed to CO_3^{2-} groups in the apatite structure are well defined [26, 27]. The carbonate bands at 1545 and 1460 cm^{-1} correspond to incorporation of CO_3^{2-} groups at the OH^- position (A-type) and those at 1460 and 1419 cm^{-1} to the occupation of PO_4^{3-} sites in the apatite structure (B-type). The band at 876 cm^{-1} is assigned to both types of incorporation [26, 27]. At a quenched temperature of 1120°C, the intensity of the band at 1419 cm^{-1} decreases. This could be interpreted as a release of carbonate from PO_4^{3-} positions in the apatite structure. With further temperature increase to 1280°C, the carbonate bands become less intense, and the OH^- bands assigned to the stretching and librational frequencies of hydroxyapatite (3571 and 631 cm^{-1}) [24] are observed.

The temperature dependence of the FTIR spectra of the gel with Ca/P = 1.77 is shown in Fig. 8. The OH^- band at 3571 cm^{-1} is observed even at 590°C, which is in accordance with the XRD analysis (Fig. 5). The bands at 1545, 1460, 1410 and 877 cm^{-1} arising from the CO_3^{2-} groups at the PO_4^{3-} positions, as well as at the OH^- positions, are well defined in the samples quenched from 900 and 1060°C.

FTIR spectra of gels with various Ca/P molar ratios sintered at 1000°C for 3 hours are shown in Fig. 9. All of the gels except that with Ca/P = 1.56 exhibit the absorption bands characteristic of OH^- groups in hydroxyapatite (3571 cm^{-1} and 631 cm^{-1}). The absorption bands attributed to CO_3^{2-} groups incorporated at the OH^- positions are stronger in the spectra of samples with CA/P $\leq$ 1.66, whereas the bands attributed to CO_3^{2-} groups substituting PO_4^{3-} tetrahedra are stronger in the gels with molar ratios Ca/P $\geq$ 1.70. Additionally, in the EHP6 gel (Ca/P = 1.77), the band at 3643 cm^{-1} attributed to $Ca(OH)_2$ [28] is also observed.

3.2. Dip-coatings on Si wafers and Ti-alloy substrates

Titanium alloy substrates (Ti-30Nb-3Al and Ti-5Al-2.5Fe) and the Si single-crystal wafers were dip coated with the prepared sols and isothermally heat treated at temperatures between 400°C and 900°C for 10 minutes. XRD patterns of EHP3 (Ca/P = 1.62) coatings on Si wafers and on Ti-5Al-2.5Fe substrates sintered in air are shown in Fig. 10. HAP started to form at 500°C either on Si wafer or on Ti-alloy substrate. Further increase in heat-treatment temperatures induces the formation of small amount of β-TCP, which disappears at 800°C. Ti-alloy substrate started to oxidize at 700°C. At 800°C rutile (TiO_2) is the major phase, and small intensity peaks at 36.68°, 42.68° and 62° 2θ (see Fig. 10C)

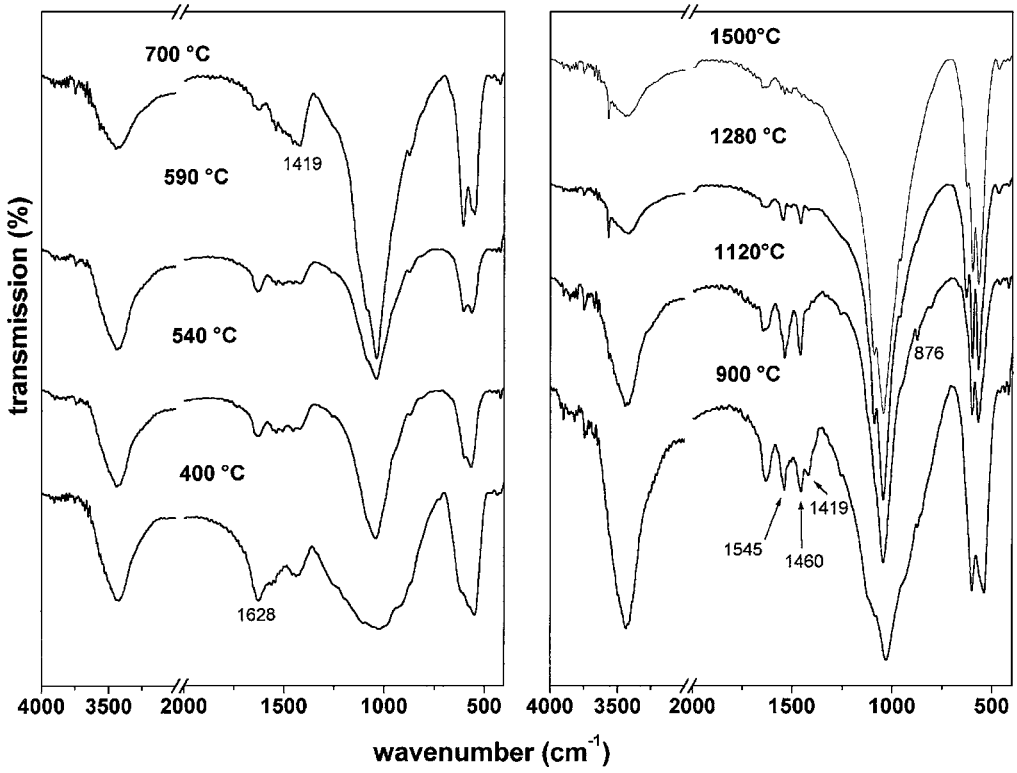

Figure 7 FTIR spectra of EHP3 gel (Ca/P = 1.62) quenched in the DTA from the temperatures marked in Fig. 3.

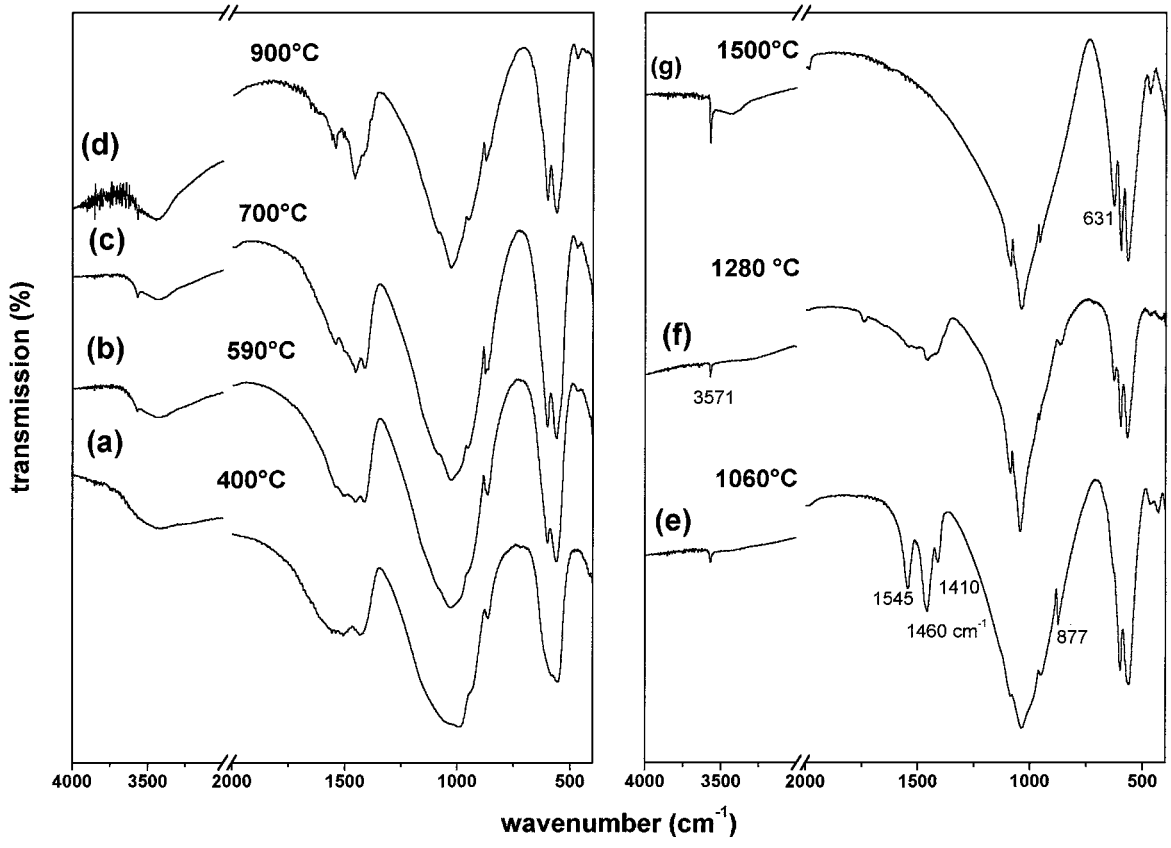

Figure 8 FTIR spectra of EHP6 gel (Ca/P = 1.77) quenched in the DTA from the marked temperatures.

on XRD pattern of the sample could be assigned to the intermediate phase TiO_x with $x \approx 1$. At 900°C, there is no other titanium oxide phase but rutile.

Fig. 11 displays XRD patterns and FTIR spectra of dip-coatings on Si wafers sintered at 600°C in air. The peaks in the XRD patterns (see Fig. 11A) are very broad, which suggests the existence of small primary particles. In the coating with Ca/P = 1.56 (pattern c), β-TCP is the main phase, with small amounts of HAP and carbonate apatite. However, in the coating with Ca/P = 1.62

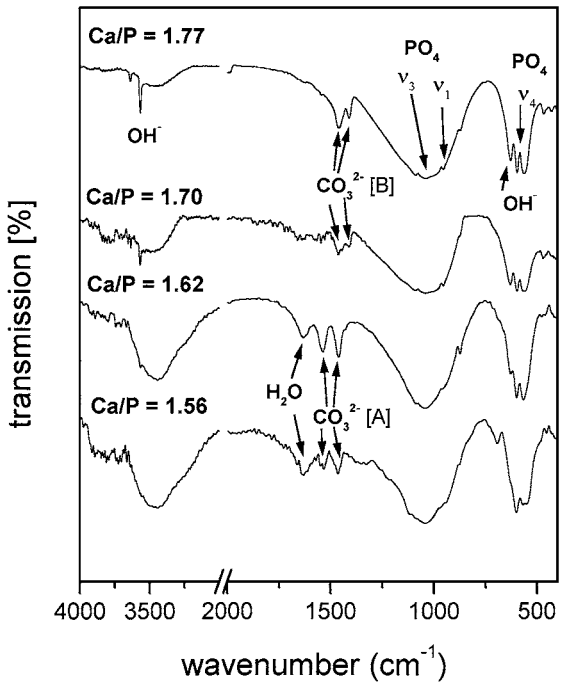

Figure 9 FTIR spectra of EHP1, EHP3, EHP5 and EHP6 gels heat treated at 1000°C for 3 hours.

(pattern b), HAP is the major phase and β-TCP is present in a smaller amount, and for Ca/P = 1.77 (pattern a), the former is the only phase formed at 600°C.

In the FTIR spectra of Fig. 11B, no absorption bands of OH^- groups characteristic for the presence of hydroxyapatite are observed. Small carbonate bands at 1455 and 1410 cm^{-1}—attributable to B-type substitution of CO_3^{2-} groups—are found in the EHP6 coating (spectrum *a*). In EHP1 coating (Ca/P = 1.56) (spectrum *c*), PO_4^{3-} bands characteristic for β–TCP at 947 and 974 cm^{-1} are evident [29], and bands belonging to organic residuals as well as to carbonate ions incorporated into the structure are also visible.

SEM micrographs of coatings on a Ti-5Al-2.5Fe substrate and a Si wafer are shown in Fig. 12A and B, respectively. They reveal that homogeneous and dense films with thickness of 250 nm are obtained by dip coating and sintering in two cycles.

4. Discussion

4.1. Thermal behavior of prepared sols

Thermoanalytical investigations performed on as-dried gels having Ca/P molar ratios between 1.56 and 1.77

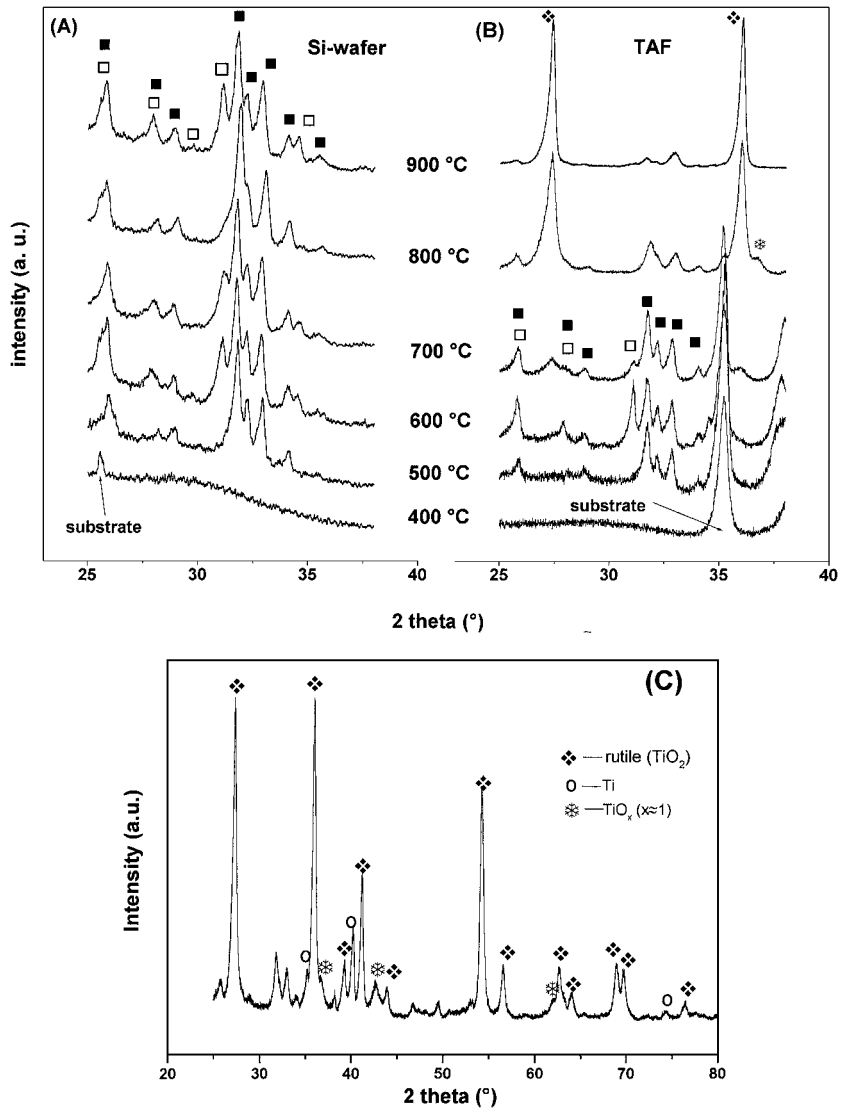

Figure 10 XRD patterns taken from the surface of sol-gel derived coatings: (A) on Si wafers, (B)- on Ti-5Al-2.5Fe alloys (TAF) sintered at the indicated temperatures, (C) XRD pattern of coating on TAF at 800°C in the 2θ range of 24–80°. Rutile and TiO_x ($x \approx 1$) are formed at the coating/substrate interface. (—□—) β-TCP; (—■—) hydroxyapatite; (—❖—) rutile (TiO_2); ❄ TiO_x ($x \approx 1$); o Ti.

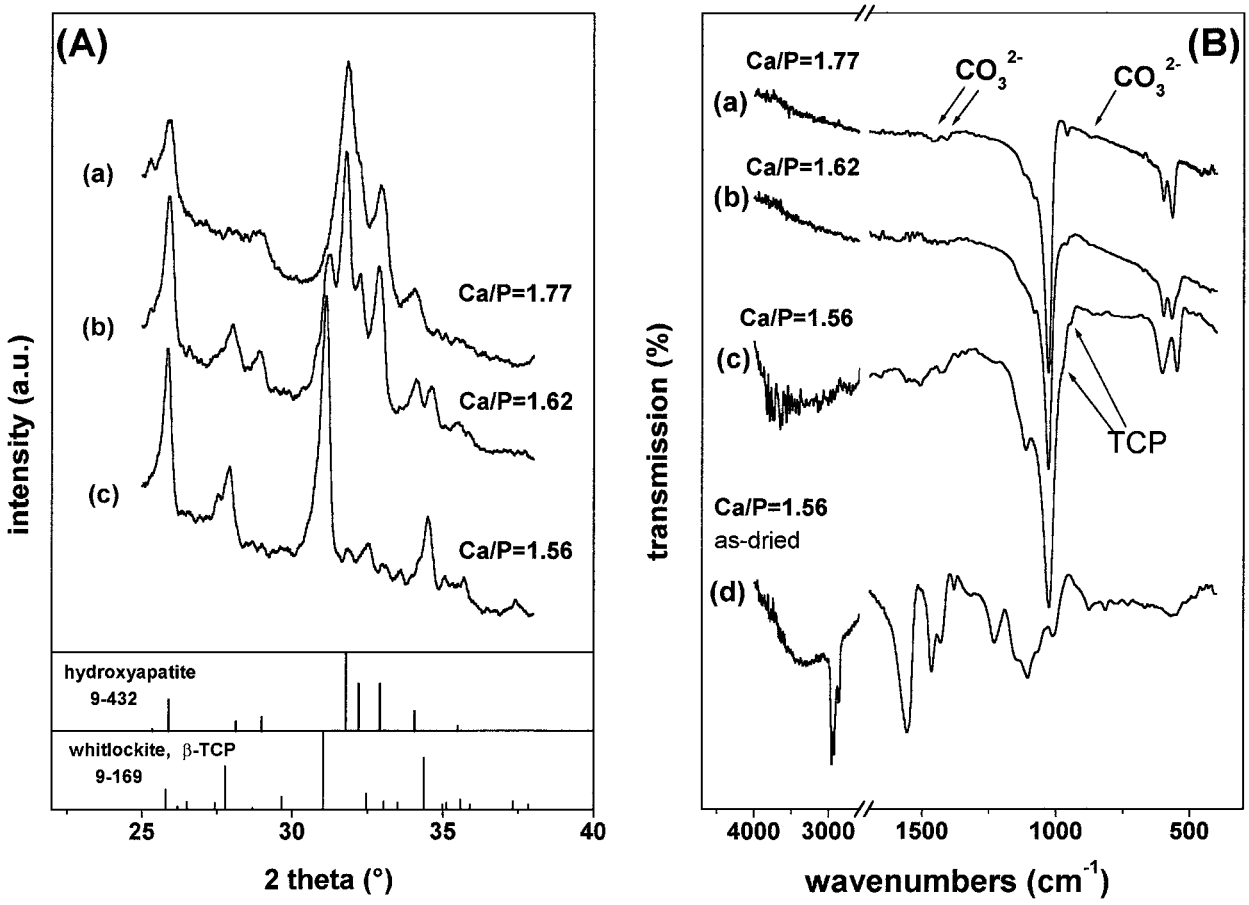

Figure 11 (A) XRD patterns and (B) FTIR spectra of dip-coatings with different Ca/P molar ratio sintered at 600°C for 10 minutes on Si-wafers: (a) Ca/P = 1.77; (b) Ca/P = 1.62; (c) Ca/P = 1.56 and (d) spectrum of as-dried gel with Ca/P = 1.56.

reveal that the organic component of the gels decomposes nearly completely at about 400°C, exhibiting a strong exothermic DTA peak (Fig. 2) that is characteristic of burn-off processes. However, when the gels are momentarily brought to a sintering temperature of 400°C and held there for only 5 minutes, the organic is burned off only partially. When such a pre-heated sample is submitted to thermal analysis, the organic rest decomposes in three different temperature ranges (500–700°C, 900–1120°C and 1120–1280°C) (Fig. 3). The samples quenched at 400°C are amorphous, but crystallization of calcium phosphates (and carbonate phosphate) takes place upon annealing at higher temperatures. These crystallization reactions occur simultaneously with the above mentioned organic burn-off processes, since the samples quenched from 400°C are still amorphous, and all of the small exothermic peaks seen in DTA scan at higher temperatures (Fig. 2) are accompanied by weight loss as is evident in the TGA curve of Fig. 3.

Whether solely HAP or a mixture of HAP and β-TCP crystallize during the heat treatment of gels depends on the Ca/P molar ratio. We expected to find the formation of HAP with a small amount of TCP in the system with Ca/P = 1.62, however, the powder calcined at 700°C contained β-TCP as the major phase and poorly crystalline HAP as a minor one (Fig. 4). The unexpectedly large amount of β-TCP likely results from the different decomposition rates of calcium and phosphorus precursors. Since the Ca/P molar ratio of TCP equals 1.50, it is necessary to assume, for stoichiometric reasons, that the HAP has a Ca/P molar ratio distinctly greater than 1.67, suggesting the incorporation of foreign anions in the HAP structure. FTIR spectra provide an important due to the nature of these anions, since all spectra recorded on the calcined gels (in the temperature range 500–1280°C) show some absorption bands of carbonate (Figs 7 and 8). The formation of carbonate ions can be attributed to the presence of organic residuals in the system, which oxidize and form carbonate ions within the HAP lattice.

Above 900°C and at Ca/P $\leq$ 1.67 molar ratios, carbonate apatite ($Ca_{10}(PO_4)_6CO_3$) forms as an additional intermediate phase (Figs 4 and 6). There exists an ambiguity regarding the molecular formula of carbonate apatite [26]. We assume that some OH^- groups can be incorporated in its structure and that the formula $Ca_{10}(PO_4)_6[(OH)_{2-2y}(CO_3)_y]$ better describes carbonate apatite. It is stable in a rather narrow temperature range between ~900 and ~1200°C under the experimental conditions described above, since, at 900°C the largest peak of carbonate apatite is evident in an XRD pattern as a shoulder on the left side of hydroxyapatite diffraction peak at $2\theta = 31.7°$ (Fig. 4). At 1120°C, the peaks of carbonate apatite are easily identifiable, and at 1280°C, they completely disappear. Varying the heat-treatment of gels at 1000°C also influences the amount of carbonate apatite in calcined powders (Fig. 6). Calcining the gel with Ca/P = 1.62 at 400°C for 1 h before heat-treatment at 1000°C caused

a decrease in the amount of carbonate apatite, because of a decrease in carbon content at 400°C.

In the gels with Ca/P ≥ 1.70, no carbonate apatite forms as a separate phase above 900°C, but some splitting of HAP peaks is found in the XRD pattern at 1060°C (Fig. 5B). The first set of peaks corresponds well to the theoretical values for HAP (JCPDS 9-432), whereas the second set is shifted to smaller 2θ values (Fig. 5B). This suggests the presence of an intermediate HAP phase with a lower crystal symmetry than that of stoichiometrical $Ca_{10}(PO_4)_6(OH)_2$.

The FTIR spectra presented in Figs 7–9 provide further detail regarding the structure of investigated powders. According to Refs. [26, 27], CO_3^{2-} can substitute OH^- groups in hydroxyapatite (A-type sites), or CO_3^{2-} can be incorporated at the positions of PO_4^{3-} tetrahedral groups in the apatite structure (B-type sites). The differentiation between these two sites is possible through infrared studies, with principal bands of CO_3^{2-} groups occurring at 1460 and 1540 cm^{-1} for A sites, and 1460 and 1410 cm^{-1} for B sites. The band at 876 cm^{-1} is assigned to both types of substitutions.

These results suggest that the incorporation of CO_2 in the HAP formed below 700°C is not well defined (Figs 7 and 8). We refer to this HAP as **carbonate-containing HAP**. The incorporation of CO_2 at distinct PO_4^{3-} and OH^- positions of HAP is well defined at 900 and 1060°C. According to Ref. [29], this HAP is referred to as **AB-carbonated hydroxyapatite**. If **carbonate apatite** is determined by XRD as a distinct phase (the gels with CaP ≤ 1.67), the predominance of CO_2 incorporation in the OH^- positions of apatite is observed (Figs 4 and 6). On the other hand, in the gels with Ca/P ≥ 1.70, CO_3^{2-} incorporation at the PO_4^{3-} positions is dominant, although some OH^- groups are also replaced by CO_3^{2-} anions (Figs 8 and 9).

On the basis of the thermal behaviour of the investigated systems, we propose the following crystallization path in the gels with molar ratio Ca/P ≤ 1.67: β-TCP and nanocrystalline **carbonate-containing hydroxyapatite** crystallize above 500°C. At $T \geq 700$°C both phases react with each other, forming **AB-carbonated hydroxyapatite**, following reaction (1). The latter phase has been described by Layrolle *et al*. [29] using the formula $Ca_{10-2x/3}[(PO_4)_{6-x}(CO_3)_x][(OH)_{2-x/3-2y}(CO_3)_y]$. The Ca/P molar ratio of AB-carbonated hydroxyapatite is greater than 1.67 for any value of $x (0 < x < 6)$, i.e., regardless of the amount of carbonate that replaces the phosphate groups. We assume the same formula for carbonate containing and for AB-carbonated HAP, but with different x values. For stoichiometrical reasons the latter phase should have a lower Ca/P ratio than the former one, because the relative amount of β-TCP decreases with temperature. This process ends with the formation of **carbonate apatite** $Ca_{10}(PO_4)_6[(OH)_{2-2y}(CO_3)_y]$ following reaction (2). At $T \sim 1200$°C carbonate apatite begins to decompose into HAP according to reaction (3). (In the FTIR spectrum at 1280°C in Fig. 7, distinct OH^- vibrations are observed at 3571 cm^{-1} and 631 cm^{-1}). At $T > 1280$°C β-TCP transforms into α-TCP [30].

$$\beta\text{-}Ca_3(PO_4)_2 + \text{nanocrystalline, carbonate-containing hydroxyapatite} \longrightarrow \xrightarrow{700-900^\circ C} \underset{\text{AB-carbonated HAP}}{Ca_{10-2x/3}[(PO_4)_{6-x}(CO_3)_x][(OH)_{2-x/3-2y}(CO_3)_y]} \quad (1)$$

$$\underset{\text{AB-carbonated HAP}}{Ca_{10-2x/3}[(PO_4)_{6-x}(CO_3)_x][(OH)_{2-x/3-2y}(CO_3)_y]} \xrightarrow[-CO_2\,(\text{in } x \text{ position})]{900-1100^\circ C} \underset{\text{carbonate apatite (A substitution)}}{Ca_{10}(PO_4)_6[(OH)_{2-2y}(CO_3)_y]} + CO_2\downarrow \quad (2)$$

$$\underset{\text{carbonate apatite}}{Ca_{10}(PO_4)_6[(OH)_{2-2y}(CO_3)_y]} \xrightarrow[\substack{-CO_2\,(\text{in } y \text{ position})\\ +H_2O\,(\text{atm.})}]{\sim 1200^\circ C} \underset{\text{HAP}}{Ca_{10}(PO_4)_6(OH)_2} + CO_2\downarrow \quad (3)$$

In the systems with excess calcium (Ca/P ≥ 1.70), the presence of AB-carbonated hydroxyapatite—with CO_3^{2-} predominantly incorporated on PO_4^{3-} positions and only partially on OH^- positions—should be assumed at 700°C. (OH^--stretching vibrations at 3571 cm^{-1} characteristic of hydroxyapatite are observed at 700°C; Fig. 8). The β-TCP content is smaller than in the systems with Ca/P ≤ 1.67. Its decrease with temperature is accompanied by a decrease in the Ca/P molar ratio of AB-carbonated hydroxyapatite and by some evolution of CO_2 from A positions in the HAP structure. We assume that this process ends with the formation of an intermediate phase, referred to as **B-carbonated hydroxyapatite** ($Ca_{10-2x/3}[(PO_4)_{6-x}(CO_3)_x](OH)_{2-2x/3}$ [29]), following the reaction (4). (CO_3^{2-} ions are seen at PO_4^{3-}positions even at 1060°C; Fig. 8 spectrum e). The transformation of B-carbonated hydroxyapatite into stoichiometrical HAP is proposed in reaction (5). The splitting of the XRD peaks of HAP seen in Fig. 5B could be explained by lower symmetry of B-carbonated hydroxyapatite. Since the overall Ca/P molar ratio is higher than 1.67, after total evolution of CO_2 at $T > 1280$°C, the excess Ca ions crystallize as calcium oxide (Fig. 5). Absorption of atmospheric water through CaO after cooling down explains the OH^--stretching bands at 3643 cm^{-1} in the FTIR spectra of calcined powders (Fig. 9).

$$\underset{\text{AB-carbonated HAP}}{Ca_{10-2x/3}[(PO_4)_{6-x}(CO_3)_x][(OH)_{2-x/3-2y}(CO_3)_y]} \xrightarrow[\substack{-CO_2(\text{in } y\text{position})\\ +H_2O(\text{atm.})}]{>700^\circ C}$$

$$\longrightarrow \underset{\text{B-carbonated HAP}}{Ca_{10-2x/3}[(PO_4)_{6-x}(CO_3)_x](OH)_{2-2x/3}} + CO_2 \uparrow \quad (4)$$

$$\underset{\text{B-carbonated HAP}}{Ca_{10-2x/3}[(PO_4)_{6-x}(CO_3)_x](OH)_{2-2x/3}} \xrightarrow[-CO_2(\text{in } x \text{ position})]{>1200^\circ C} \underset{\text{HAP}}{Ca_{10}(PO_4)_6(OH)_2} + CO_2 \uparrow + CaO \quad (5)$$

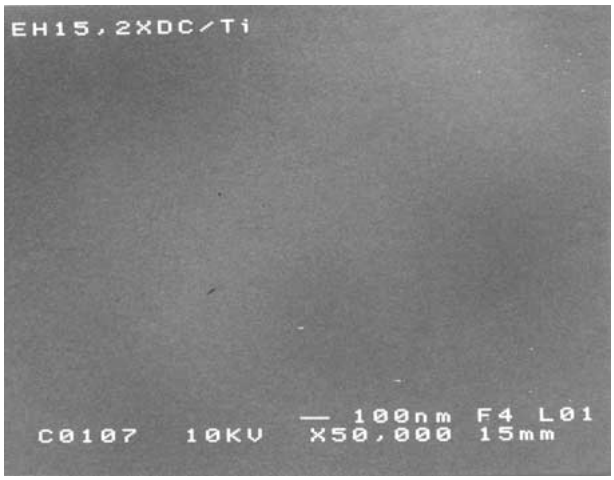

(A)

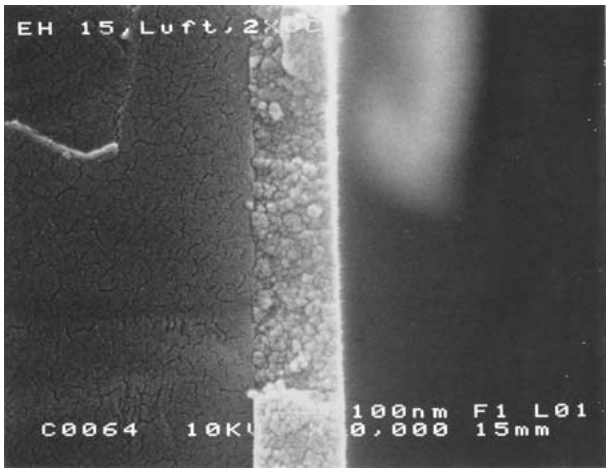

(B)

Figure 12 SEM micrographs of: (A) coated surface of Ti-5Al-2.5Fe substrate and (B) fracture surface of EHP6 film on Si.

4.2. Coatings on Si wafers and Ti-alloy substrates

It is quite obvious that the evolution of crystalline phases in coatings is somewhat different (Fig. 10) than in the same gel heated without a substrate (Fig. 4), since the coatings are brought rapidly to the sinter temperature and are densified in a short time, in order to avoid deterioration of the mechanical properties of the substrates. Generally, it can be said that there is no difference in the crystallization path of coatings on Si wafers and on Ti-alloy substrates, except that the oxidation of the latter occurred above 600°C. Small amount of rutile (TiO_2) was detected at 700°C, and at 800°C that is the major titanium oxide phase.

Three small peaks at $2\theta^{\circ}_{Cuk_\alpha} = 36.68, 42.68$ and 62.00 (Fig. 10C) could be attributed to TiO_x phase (with $x \approx 1.04$). Compared with the standard peaks of $TiO_{1.04}$ (JCPDS 43-1296) these peaks are shifted downward by about 0.7° 2θ (Cu K_α), which could be due to a difference in stoichiometry of this cubic phase. The formation of $TiO_x (x \approx 1.04)$ as a major phase rather than rutile was observed by Park and Condrate [31]. They also observed shift of peaks downward by about 0.5° 2θ (Cu K_α) in the comparison to $TiO_{1.04}$ phase. As the difference to our experiment (sintering in air) they prepared coatings by plasma spraying using inert/reducing primary gas, consequently, they greatly reduced the oxidation of substrate and rutile formation. The formation of $TiO_x (x \approx 1)$ in our experiment is observed only at 800°C and the end product of the substrate oxidation is rutile. Changes in the amount of β-TCP from 500 to 700°C (seen in coatings on Si-wafer, as well as on TAF) are explained by reaction (1), while changes in the phase composition at $T > 800$°C are induced by reactions of substrate with the coating phases, such as the reaction of rutile with hydroxyapatite (6), which explains the formation of β-TCP at 900°C:

$$TiO_2 + Ca_{10}(PO_4)_6(OH_2) \xrightarrow{>700^\circ C} CaTiO_3 + 3Ca_3(PO_4)_2 + H_2O \quad (6)$$

A similar reaction may occur between SiO_2, formed by the oxidation of the Si wafer, and the HAP coating. Sintering at 600°C for 10 minutes was found to be the optimum for coatings on the Ti-alloy substrates.

Although a carbonate apatite could not be determined in the coatings, as a distinct phase, the absorption bands characteristic of CO_3^{2-} anions incorporated at OH^- positions are small but discernible and independent of Ca/P ratio (Fig. 11). The only phase detected in a coating of EHP6 (Ca/P = 1.77) is B-carbonated HAP, whereas in an EHP3 (Ca/P = 1.62) coating AB-carbonated HAP and β-TCP are observed, and in a coating of EHP1 (Ca/P = 1.56) β-TCP is found along with traces of HAP.

The microstructural observations (SEM micrographs in Fig. 12A and B) clearly demonstrate that sol-gel-derived HAP coatings provide very uniform and homogeneous films on substrates, the thickness of which can be controlled by the number of dip-coatings. In Fig. 12B

the thickness of two dip-coated films on a Ti-5Al-2.5Fe substrate sintered at 600°C amounts 250 nm.

5. Conclusion

(1) HAP powders prepared by the sol-gel technique using calcium 2-ethylhexanoate ($Ca(O_2C_8H_{15})_2$) as calcium precursor and 2-ethyl-hexyl-phosphate as phosphorus precursor always contain a certain amount of carbonate anions, which can be incorporated in the structure of hydroxyapatite at two different positions.

(2) The position of the carbonate anions depends on the Ca/P molar ratio and the sintering temperature of the gels.

(3) If $Ca/P \leq 1.67$, CO_3^{2-}groups substitute both PO_4^{3-}tetrahedra and OH^--groups in the HAP structure forming so called AB-carbonated HAP. Carbonate anions substituting PO_4^{3-}groups in the structure are released between ∼900 and ∼1200°C, forming carbonate apatite. The latter phase further transforms into HAP above 1200°C.

(4) If $Ca/P \geq 1.70$, CO_3^{2-}groups substitute predominantly the PO_4^{3-}positions in HAP and to a lesser extent, the OH^- positions, forming an AB-carbonated hydroxyapatite with a greater CO_3^{2-} occupancy of B positions. Formation of intermediate B-carbonated hydroxyapatite rather than carbonate apatite explains the splitting of *hkl* reflections observed by XRD. After total evolution of CO_2 from the structure at $T > 1280$°C, the excess calcium is present as calcium oxide or as $Ca(OH)_2$.

(5) The gels form very uniform and homogeneous films on substrates, the thickness of which is controlled by the number of dip-coatings. The thickness of two layers on a Ti-5Al-2.5Fe substrate sintered at 600°C amounted to 250 nm.

References

1. R. J. FURLONG and J. F. OSBORN, *J. Bone Joint Surg.* **5** (1991) 741.
2. R. EVASIC, *Dentistry Todays* **2** (1993) 90.
3. P. DUCHEYNE, S. RADIN, M. HEUGHEBAERT and J. C. HEUGHEBAERT, *Biomaterials* **11** (1990) 244.
4. D. M. LIU, H. M. CHOU and J. D. WU, *J. Mater. Sci.: Mater. Med.* **5** (1994) 147.
5. L. Z. LeGEROS, J. P. LeGEROS, R. KIJKOWSKA, R. ZHENF, C. BAPTISTA and J. L. WONG, in "Ceramic Transactions, Vol. 48. Bioceramics: Materials and Applications," edited by G. Fischman, A. Clare and L. Hench (American Ceramic Society, Westerville, OH, 1995) p. 173.
6. R. D. BLOEBAUM, D. A. BEEKS, L. D. DORR, J. A. DUPONT, C. G. SAVORY and A. A. HOFMAN, Proceedings of the 20th Annual Meeting of the Society for Biomaterials, Boston, MA, 1994 (Society for Biomaterials, Mineapolis, MN, 1994) p. 125.
7. L. TORISSI and G. FOTI, *Appl. Phys. Lett.* **62** (1993) 237.
8. C. M. COTELL, *Appl. Surf. Sci.* **69** (1993) 140.
9. Y. FUJISHIRO, T. SATO and A. OKUWAKI, *J. Mater. Sci.: Mater. Med.* **6** (1995) 172.
10. M. TANACHASHI, T. YAO, T. KOKUBO, M. MINODA, T. NAKAMURA and T. YAMAMURA, *ibid.* **6** (1995) 319.
11. T. KOKUBO, K. HATA, T. NAKAMURA and T. YAMAMURO, in "Bioceramics," Vol. 4 edited by W. Bonfield, G. W. Hasting and K. E. Tanner (Butherworth Heinemann Ltd., 1991) p. 113.
12. H. B. WEN, J. R. De WIJN, Q. LIU, K. De GROOT and F. Z. CUI, *J. Mater. Sci.: Mater. Med.* **8** (1997) 765.
13. C. J. BRINKER and G. W. SCHERRER, "Sol-Gel Science: The Physics and Chemistry of Sol-Gel Processing" (Academic Press, New York, 1992) p. 845.
14. A. DEPTULA, J. REBANDEL, W. DROZDA, W. LADA and T. OLCZAK, in "Better Ceramics Through Chemistry," edited by V. M. J. Hampden-Smith, W. G. Klemperer and C. J. Brinnker (*Mat. Res. Soc. Symp. Proc.* 270, Pittsburgh, PA, 1992) p. 277.
15. Y. MASUDA, K. MATUBARAAND and S. SAKKA, *J. Ceram. Sco. Jpn.* **98** (1990) 84.
16. T. BRENDEL, A. ENGEL and C. RUESSEL, *J. Mater. Sci.: Mater. Med.* **3** (1992) 175.
17. Q. QUII, P. VINCENT, B. LOWENBERG, M. SAYER and J. E. DAVIES, *Cells Mater.* **3** (1993) 351.
18. W. WENG and J. P. BAPTISTA, *J. Am. Ceram. Soc.* **82** (1999) 27.
19. C. M. LOPATIN, T. L. ALFORD, V. B. PIZZICONI and T. LAURSEN, *Mater. Letters* **37** (1998) 211.
20. S. W. RUSSELL, K. A. LUPTAK, C. T. A. SUCHICITAL, T. L. ALFORD and V. B. PIZZICONI, *J. Am. Ceram. Soc.* **79** (1996) 837.
21. M. SAUER, R. NONNINGER and H. SCHMIDT, in Werkstoffwoche '98, Werstoffe für Medizintechnik Band IV Symp. 4, editors H. Planck and H. Stallforth (Wiley-VCH, Weinheim, New York, 1999) p. 67.
22. M. HOSONUMA and T. SHIMAMUNE, "Process for producing metal composite materials having a coating of calcium phosphate for bone and tooth implants," Patent EP 310574 A1 19890405 EP 88-830391 19880928.
23. I. C. ISON, M. T. FULMER, B. M. BARR and B. R. CONSTANTZ, in "Hydroxyapatite and related materials," editors P. W. Brown and B. Constantz (CRC Press, 1994) p. 215.
24. I. REHMAN and W. BONFIELD, *J. Mater. Sci.: Mater. Med.* **8** (1997) 1.
25. P. LAYROLLE and A. LEBUGLE, *Chem. Mater.* **6** (1994) 1996.
26. B. NARASARAJU and D. E. PHEBE, *J. Mater. Sci.* **31** (1996) 1.
27. SUETSUGU, I. SHIMOYA and J. TANAKA, *J. Am. Ceram. Soc.* **81** (1998) 746.
28. R. RAO, H. N. ROOPA and T. S. KANNAN, *J. Mater. Sci.: Mater. Med.* **8** (1997) 511.
29. P. LAYROLLE, A. ITO and T. TATEISHI, *J. Am. Ceram. Soc.* **81** (1998) 1421.
30. A. TAMPIERI, G. CELOTTI, F. SZONTAGH and E. LANDI, *J. Mater. Sci.: Mater. Med.* **8** (1997) 29.
31. E. PARK and R. A. CONDRATE Sr., *Mater. Letters* **40** (1999) 228.

Received 11 April 2000
and accepted 4 May 2001